

Synthesis and Antibacterial Activity of Azomethine Ligand and Their Metal Complexes: A Combined Experimental and Theoretical Study

Khalidah Hamil Manati Al Furaiji, Rehab Abdul Mahdi Al Hassani, and Hanaa Hassan Hussein*

Department of Chemistry, College of Science, Mustansiriyah University, Baghdad 10052, Iraq

* Corresponding author:

email:

albajalanhanaa@uomustansiriya.edu.iq

Received: March 30, 2023

Accepted: May 11, 2023

DOI: 10.22146/ijc.83508

Abstract: An asymmetrical Schiff base triazole ligand (4-((3-mercapto-5-(naphthalen-1-ylmethyl)-4H-1,2,4-triazol-4-yl)imino)methyl)methoxy) (L) was used to generate novel micro complexes of Cr(III), VO(IV), and Mn(II) ions. Different spectroscopic techniques, including UV-vis spectroscopy, Fourier transform infrared spectroscopy (FTIR), flame atomic absorption, conductivity tests, CHNS elemental analysis, and magnetic susceptibility, were used to determine the structures of the Schiff base micro complexes. The density functional theory (DFT) calculation was screened to consider selected complexes. The observed data indicated their stability, and the expected chemical formula of vanadium(IV) was square pyramidal geometry in VO(L) complex formula. In contrast, the Cr(III) and Mn(II) complexes have octahedral geometry in the formulas. Frontier molecular orbitals calculations (MO) have also been performed to better understand the nature of orbitals, E_{HOMO} , and E_{LUMO} , allowing us to confirm the experimental finding. *Pseudomonas aeruginosa* and *Bacillus subtilis*, two types of potentially dangerous bacteria, were subjected to tests to see whether L and its metal complexes have any antibacterial activities or not. All compounds were also tested for their antifungal activity against two different types of fungi, *Penicillium spp.* and *Aspergillus flavus*. There is significant action has been noted in all cases for the complexes.

Keywords: Schiff base; DFT; transition-metal; antibacterial activity

■ INTRODUCTION

Some physical and chemical features of heterocyclic compounds are affected by heteroatoms [1]. Several organic heterocyclic compounds belonged to the triazole family. Triazole has a di-unsaturated ring structure with three nitrogen atoms and two carbon atoms at a non-adjacent site, and there are five members in this class. Triazole derivatives, which include the significant family of heterocyclic compounds known as pyrrodiazole, are also known by that name. Natural triazole is employed in numerous critical items [2-4], such as hormones, vitamins, pigments, and antibiotics. It is common practice to use Schiff base ligands for stabilizing metals in a variety of oxidation states and for adjusting metal behavior in catalysis [5]. Thus, over the past decade, computational investigation of Schiff base triazole ligand reactions with transition elements has emphasized using density

functional theory (DFT) theoretical methods to explore their molecular structures, spectroscopic properties, orbitals distributions, and antibacterial activities [6].

It was discovered that metal complexes, in contrast to their parent ligands, demonstrated a higher level of biological activities as a result of chelation [4]. DFT was also employed to further study 3d transition-metal methoxide complexes with potentially redox-no innocent pincer-supporting ligands. Methane activation reaction mechanism and metal identity influence on thermodynamics and kinetics were elucidated using three tridentate pincers and several first-row transition metals (M = Mn, Ti, Cr, Ni, V, Co, Cu, and Fe) [5]. The data at hand enables the description of processes, especially those incorporating transition metals, using DFT and *ab initio* molecular orbital techniques [6].

Koga and Morokuma [7] provide a summary of this

topic. Two recent reviews of theoretical updates to transition-metal chemical reactions are provided by Musaev and Morokuma [8] and Siegbahn and Blomberg [9]. The research of Salahub et al. [10] and Ellouz et al. [11] analyzed DFT methods and their implementations to transition-metal reactions. Due to practical developments, this work has gained significant interest as a comprehensive review of the concepts of biologically active molecules [12].

The mercapto- and thione-substituted 1,2,4-triazole ring structures are two types of 1,2,4-triazole derivatives that have been investigated for their diverse biological features. Antioxidant properties are included within these substances [13-14]. Schiff base 1,2,4-triazole-2-thione compounds have the N=C and the C=S groups as characteristic chromophores, mainly used in biopharmacological activities and advanced applications in organic synthesis [15-17]. Thin (C=S) and the nitrogen of azomethine (N=CH) as a bidentate ligand allow the coordination of transition metals, resulting in a stable five-member ring [18-20]. The synthesis of their metal complexes has received significant interest [21-30] because of their wide use in medicine.

In this study, a new Schiff base 1,2,4-triazole-2-thione ligand (L) was synthesized in an effort to incorporate an azomethine moiety into the structure of a 1,2,4-triazole-2-thione ring. This allowed the study of the coordination behavior of the new ligand toward some metal ions, including Cr(III), VO(IV), and Mn(II) ions, both experimental and theoretical methods. In order to investigate the potency of L and its metal complexes with the primary ring structure to serve as an inhibitor with certain kinds of bacteria, the biological activity of L has also been taken into consideration.

■ EXPERIMENTAL SECTION

Materials

The chemicals used to synthesize were obtained from mercantile sources. All the reagents and solvents were of analytical or chemically pure grade. Methanol absolute (CH₃OH 99.5%) and ethanol absolute (C₂H₅OH 99.5%) were purchased from Sigma Aldrich (St. Louis,

MO, USA). Petroleum ether (b.p. 40–70) - 99 Fluke (Bucks, Switzerland), chromium(III) chloride, manganese(II) chloride and vanadium sulfate were obtained from Merck. All the reagents were weighed with an accuracy of ± 0.0001 g.

Instrumentation

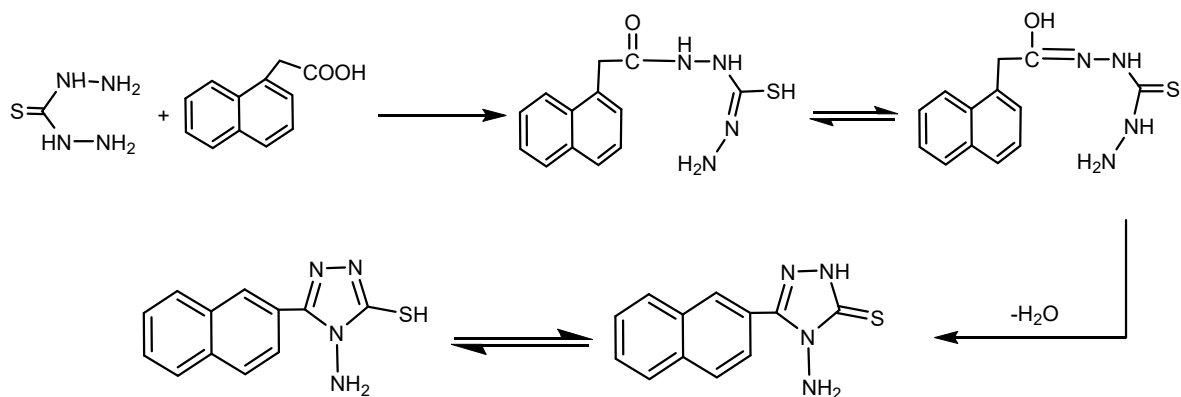
Gallenkamp MF B600 instrument was used to record melting points. EA-034.mth was used to design elemental analyses for legend and its complexes. Flame atomic absorption (Shimadzu-670 Atomic Absorption Spectrophotometer) was used to estimate metal contents. The infra-red spectra were detailed for all complexes using an 8400 S-FTIR Shimadzu spectrophotometer. Electrolytic conductivity calculating set mode (MC-1-Mark V) was used to measure molar conductivity. The magnetic susceptibility balance of Sherwood Scientific was used to measure the magnetic susceptibilities of the complex. Electronic spectra ultraviolet-visible were obtained using an 1800-UV Shimadzu spectrophotometer. The ¹H- and ¹³C-NMR spectra were conducted by 400 MHz MR spectrometer Bruker, Germany, using the internal standard tetramethylsilane and dimethyl sulfoxide (DMSO-*d*₆) as a solvent.

Procedure

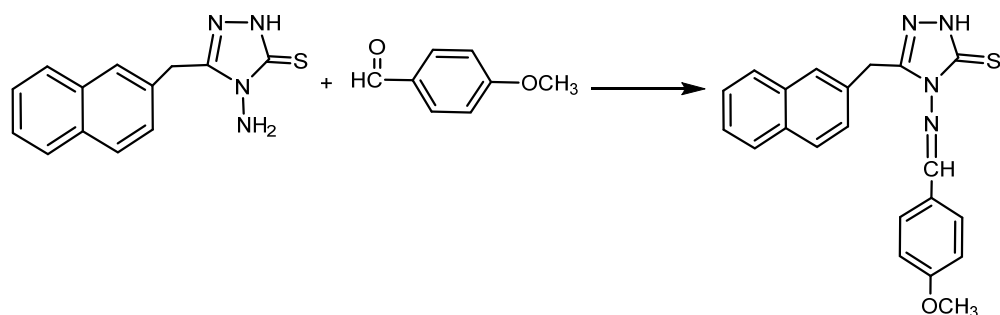
Synthesis of L

The synthetic path followed by different procedures and modified methods were used to prepare the label compounds.

TRZ (4-amino-5(naphthalene-1-ylmethyl)-4H-1,2,4-triazole-3-thiol(thione)) synthesis. The test tube containing 1.86 g (0.01 mol) of α-naphthol acetic acid and 1.59 g (0.015 mol) of thiocarbohydrazide was warmed at the melting temperature in an oil bath until its contents melted. A 5% sodium bicarbonate solution was utilized to neutralize the carboxylic acid in the final product after it was allowed to cool gradually. After forming 4-amino-5-(naphthalen-1-ylmethyl)-4H-1,2,4-triazole-3-thiol (TRZ), the substance was filtered off, washed with cold ethanol, dried at room temperature, and recrystallized from ethanol [31-32]. The strategies for synthesizing TRZ are depicted in Scheme 1.



Scheme 1. Synthesis of TRZ



Scheme 2. Synthesis of Schiff base triazole

Synthesis Schiff base triazole (4-((3-mercapto-5-(naphthalene-1-ylmethyl)-4H-1,2,4-triazole-4-yl)imino)methyl)methoxy (L).

Methanol solution of 4-methoxybenzaldehyde (1.22 g, 0.01 mol) with a few drops of glacial acetic acid and 2.56 g (0.01 mol) of TRZ was added in the round bottom flask and stirred the reaction mixture for 24 h without heating. The precipitate was filtered to extract Schiff base triazole, which was then washed with petroleum ether and crystallized again in ethanol [33-35]. Scheme 2 depicts the chemical reactions that take place.

Schiff base complexes synthesis

Ethanol solutions of appropriate MnCl_2 (0.23 g, 0.001 mmol), CrCl_3 (0.266 g, 0.1 mmol), and VO_2SO_4 (0.21 g, 0.083 mmol) metal salt were added to ethanolic solutions (0.77 g, 0.004 mol) of L at a ratio of 1:2 (metal:ligand). The mixture was then refluxed at 67 °C for 5 h. The precipitate was then filtered, washed with ethanol, and vacuum dried. The results of several chemical and physical analyses of the L and its metal complexes are shown in Table 1.

Theory and Computational Methods

All optimizations were carried out with the assistance of the Gaussian 16 computer package, Geometry [24], taking into account all compounds in the analyses. DFT using hybrid B3LYP functional [25-26] and a def2-SVP basis set were employed in the research [27]. The chemical characteristics of transition metals were better described by the UB3LYP function [28]. Single-point energy calculations at optimized geometries can be carried out to provide a more accurate treatment of electron correlation with larger basis sets [29]. The frequency calculations used to determine the static state's composition were theoretically equivalent across all three examples. By having a closer look at the frontier molecular orbital (MO) analysis based on Kohn-Sham (KS) orbitals of the highest occupied molecular orbitals (HOMO) and the lowest unoccupied molecular orbitals (LUMO), the frontier MO can be used to understand the distribution of electron density for these orbitals [30].

■ RESULTS AND DISCUSSION

Experimental Results

Physical properties of Triazole Schiff bases ligand (L) and its metal complexes

Table 1 presents the physicochemical characteristics and the analytical data of the synthesis of triazole Schiff-based ligand and its metal complexes. Synthesis of L complexes was carried out in a powder using molar ratios of 1:2 for all complexes (metal: ligand). All of the complexes have stable thermal stability and they are unaffected by the oxygen and moisture in the air. However, they were insoluble in other organic solvents except for dimethylformamide (DMF) and dimethyl sulfoxide (DMSO). The resulting value and the findings obtained from the elemental analysis agree with one another to a level that may be considered reasonable. Measurements of spectral energy and magnetic moment both provide credence to the proposed chemical formula for the molecule.

Nuclear magnetic resonance (^1H - and ^{13}C -NMR) spectra of L

Spectra of ^1H - and ^{13}C -NMR are presented in SI. The presence of an N=CH azomethine group was detected in the ^1H -NMR spectrum of L in DMSO- d_6 at a peak assignment of 9.75 ppm. The methoxy protons were also detected at 3.89 ppm while the aromatic proton signals were detected at 6.80 to 8.26 ppm. The first appearance of CH_2 protons was at 4.61 ppm, whereas the peak for the S-H group was at 13.59 ppm. On the other hand, the signal

of SH protons in the ^1H -NMR was exceedingly weak, and it was demonstrated that thiol-thione-tautomerism occurred in the ligand spectrum [31-32].

The azomethine group may be identified in the NMR spectra of L by the peak associated with N=C at 152.9 ppm. Similarly, between 118.0 and 134.5 ppm, chemical shifts were seen in aromatic carbon rings. The spectra were classified as belonging to the N-C=S/C-S thion/thiol group due to significant peaks at lower fields at 160.4 ppm. The C-O bond is associated with chemical changes at 162 ppm, the O-CH₃ bond at 66 ppm, and the CH₂ group at 29.3 ppm [36-37].

FTIR spectra of L, VOL, CrL, and MnL complexes

The FTIR analysis provided valuable insights into the complex interaction of L with the different metal ions. Based on a comparison with the values found in the literature [25], it was easy to assign the characteristic frequencies of L and its metal complexes. The spectra can be seen in SI and the data are summarized in Table 2. The L presents three bands located at 1688, 1630, and 1608 cm^{-1} corresponding to $\nu(\text{C}=\text{N})$, $\nu(\text{C}=\text{N})$, and $\delta(\text{N}-\text{H})$ for the triazole ring, respectively [18]. Also, the band which is assigned to the $\nu(\text{S}-\text{H})$ at 2645 cm^{-1} is disappeared in complexes. The bond order of carbon-sulfur increased to $\nu(\text{C}=\text{S})$ [38-39], and L basically contains estautomerism $\nu(\text{N}-\text{C}=\text{S})$ or $\nu(\text{N}=\text{C}-\text{S}-\text{H})$ groups due to thiol-thione [36-37]. The $\nu(\text{C}=\text{N})$ in the ligand L was changed to a lower wavenumber in all complexes. Nevertheless, the C=S stretching vibration

Table 1. Some analytical and physical data of L and its metal complexes

| Comp. symbol | Empirical formula | %Yield | MP* (°C) | Color | Micro elemental analyses | | | | Metal M% | (Mole ratio) |
|---|-------------------|--------|----------|--------------|--------------------------|--------|--------|-------|---------------|--------------|
| | | | | | C | S | N | H | found (calc.) | in EtOH |
| $\text{C}_{21}\text{H}_{18}\text{N}_4\text{OS}$ | L | 92 | 377 | Light Yellow | 68.01 | 8.83 | 15.03 | 5.18 | - | - |
| $[\text{VO}(\text{L})_2]\text{SO}_4$ | VOL | 85 | >350 | Dark Green | 55.92 | 10.74 | 12.48 | 4.09 | 5.80 | 1:2 |
| $[\text{Cr}(\text{L})_2\text{Cl}_2]\text{Cl}$ | CrL | 81 | >350 | Dark green | -55.33 | -10.54 | -12.29 | -3.95 | -5.59 | 1:2 |
| $[\text{Mn}(\text{L})_2\text{Cl}_2]$ | MnL | 90 | >350 | Dark Brown | 55.98 | 7.13 | 12.54 | 4.22 | 6.01 | 1:2 |
| | | | | | -55.59 | -7.06 | -12.35 | -3.97 | -5.74 | |
| | | | | | 57.88 | 7.67 | 13.05 | 4.42 | 6.54 | 1:2 |
| | | | | | -57.67 | -7.32 | -12.82 | -4.11 | -6.29 | |

*The ligand was melted, and all complexes were decomposed

was shifted to higher frequencies in all of its complexes. In order to create a stable five-membered chelate ring, ligand L coordinated the metal ion with the nitrogen atom of the imine group and the sulfur atom of the thiol group. This frequency shift is proof of this coordination [38-39]. These observations were further indicated by the appearance of $\nu(\text{M-S})$ and $\nu(\text{M-N})$ vibrational modes in the spectra of all synthesized L complexes, while $\nu(\text{M-Cl})$ excepting CrL and MnL, respectively, as shown in Table 2.

Electronic absorption spectra, magnetic susceptibility, and conductivity measurements

The UV-vis spectra of samples can be seen in SI. Three absorption bands at 230 (43478 cm^{-1}), 293 (34129 cm^{-1}), and 388 nm (2577 cm^{-1}) were seen in the UV-vis spectrum of L in absolute ethanol and were attributed to $\pi \rightarrow \pi^*$, $n \rightarrow \pi^*$, and $n \rightarrow \pi^*$, intra-ligand transitions, respectively [18]. The development of a new band in the visible and UV spectrums results from the complexation of L with metal ions. It was determined that M-L charge transfer and ligand field transitions were responsible for these bands. The bands of maximal absorption of complexes in chloroform are listed in Table 3, along with their respective assignments.

VOL. All three bands predicted for the ${}^2\text{B}_{2g} \rightarrow {}^2\text{E}_g$, ${}^2\text{B}_{2g} \rightarrow {}^2\text{B}_{1g}$, and ${}^2\text{B}_{2g} \rightarrow {}^2\text{A}_{1g}$ transitions were seen in the isolated oxovanadium VO(L) complex at 14084, 15384, and 24390 cm^{-1} . Square pyramidal geometry is characterized by these bands [31,39]. The magnetic moment is just slightly larger than the spin value of vanadium metal (2.01 B.M). In contrast to the conductivity test in DMF, which suggested that the complex is to be ionic, this finding shows a larger orbital contribution.

The VO(L) complex that was isolated showed all three of the bands that were predicted to appear at 14084, 15384, and 24390 cm^{-1} . The VO(L) complex that was isolated showed all three of the bands that were predicted to appear at 14084, 15384, and 24390 cm^{-1} . These bands are attributed to the ${}^2\text{B}_{2g} \rightarrow {}^2\text{E}_g$, ${}^2\text{B}_{2g} \rightarrow {}^2\text{B}_{1g}$, and ${}^2\text{B}_{2g} \rightarrow {}^2\text{A}_{1g}$ transitions. They are typical of a geometry known as square pyramidal [31,36]. The magnetic moment is slightly more significant than the spin value of the vanadium metal (2.01 B.M). The DMF conductivity measurement indicated that the complex is likely ionic, and this finding suggests that the orbital contribution is more significant than previously thought.

Table 2. The FTIR spectral data of L and its metal complexes

| Comp. | $\delta(\text{N-H})$ triazole ring | $\nu(\text{C=S})$ | $\nu(\text{C=N})$ imine group | $\nu(\text{C=N})$ triazole ring | $\nu(\text{M-N})$ | $\nu(\text{M-S})$ | $\nu(\text{M-Cl})$ |
|-------|---------------------------------------|-------------------|----------------------------------|------------------------------------|-------------------|-------------------|--------------------|
| L | 1608 | 1024, 1055 | 1688 | 1630 | | | |
| VOL | 1600 | 1097 | 1668 | 1635 | 530 | 425 | 371 |
| CrL | 1602 | 1068 | 1677 | 1632 | 528 | 444 | 368 |
| MnL | 1604 | 1179 | 1680 | 1634 | 533 | 439 | 380 |

Table 3. Electronic spectra, Magnetic moment (BM), and Conductance in (DMF) for (L) complexes

| Comp. | Max. absorption ν_{max} (cm^{-1}) | Band Assignment | Suggested geometry | μ_{eff} BM | Molar cond. $\text{S cm}^2 \text{mol}^{-1}$ |
|-------|--|---|-----------------------|--------------------------|--|
| VOL | 14084 | ${}^2\text{B}_{2g} \rightarrow {}^2\text{E}_g$ | Square pyramidal | 2.01 | 82.05 |
| | 15384 | ${}^2\text{B}_{2g} \rightarrow {}^2\text{B}_{1g}$ | | | |
| | 24390 | ${}^2\text{B}_{2g} \rightarrow {}^2\text{A}_{1g}$ | | | |
| CrL | 13333 | ${}^4\text{A}_{2g} \rightarrow {}^4\text{T}_{2g}$ | Octahedral | 3.89 | 77.86 |
| | 16493 | ${}^4\text{A}_{2g} \rightarrow {}^4\text{T}_{1g}$ | | | |
| | 29881 | ${}^4\text{A}_{2g} \rightarrow {}^4\text{T}_{1g}(\text{p})$ | | | |
| MnL | 15872 | ${}^6\text{A}_{1g} \rightarrow {}^4\text{T}_{1g}$ | Octahedral | 5.05 | 14.42 |
| | 16949 | ${}^6\text{A}_{1g} \rightarrow {}^4\text{E}_g$ | | | |
| | 19417 | ${}^6\text{A}_{1g} \rightarrow {}^4\text{T}_{1g}$ | | | |
| | 21276 | ${}^6\text{A}_{1g} \rightarrow {}^4\text{E}_g$ | | | |

CrL. The spectrum of the Cr(III) complex has three absorption bands located at 13333, 16493, and 29881 cm^{-1} . The spectrum displayed features characteristic of octahedral Cr(III) complexes [36-38]. The value obtained for pure octahedral Cr(III) complexes [21] is extremely near to the value found for the ν_2/ν_1 ratio, which is 1.33. The magnetic moment of the solid complex was determined to be 3.89 B.M. The complex's lack of conductivity in DMF demonstrated that it was not an electrolyte.

MnL. Weak absorption bands at 15872, 16949, 19417, and 21276 cm^{-1} may be seen in the Mn(II) complex UV-vis spectra, indicative of the octahedral geometry of this complex. Bands from this spectrum might be assigned to ${}^6A_{1g} \rightarrow {}^4T_{1g}$, ${}^6A_{1g} \rightarrow {}^4E_g$, ${}^6A_{1g} \rightarrow {}^4T_{1g}$, and ${}^6A_{1g} \rightarrow {}^4E_g$ transitions, respectively [31-32,39]. The value of the magnetic moment of the Mn(II) complex was 5.05 B.M, which is within the range that was predicted based on the octahedral geometry surrounding the central metal ion

[32,39-41]. Stereochemical models for metal complexes with L can be seen in Fig. 1.

Theoretical Results

Geometrical optimization (stereochemical models for metal complexes with L and its metal complexes)

To support our experimental finding, first, we scheme the geometrical optimization at the UB3LYP def2-SVP level theory of L, VOL, CrL, and MnL complexes, which can show the difference in the molecular geometries and reactivity for all compounds. As shown in Fig. 2, the result of electronic ground state energies calculations beyond the UB3LYP/def2-SVP level of theory was reported in harries for all compounds. As can be seen in Table 4, a real, local minimum for all compounds due to the imaginary frequencies having zero values. Our computed geometrical parameters with b3lyp/def2-SVP theory level are in good agreement with experimentally reported

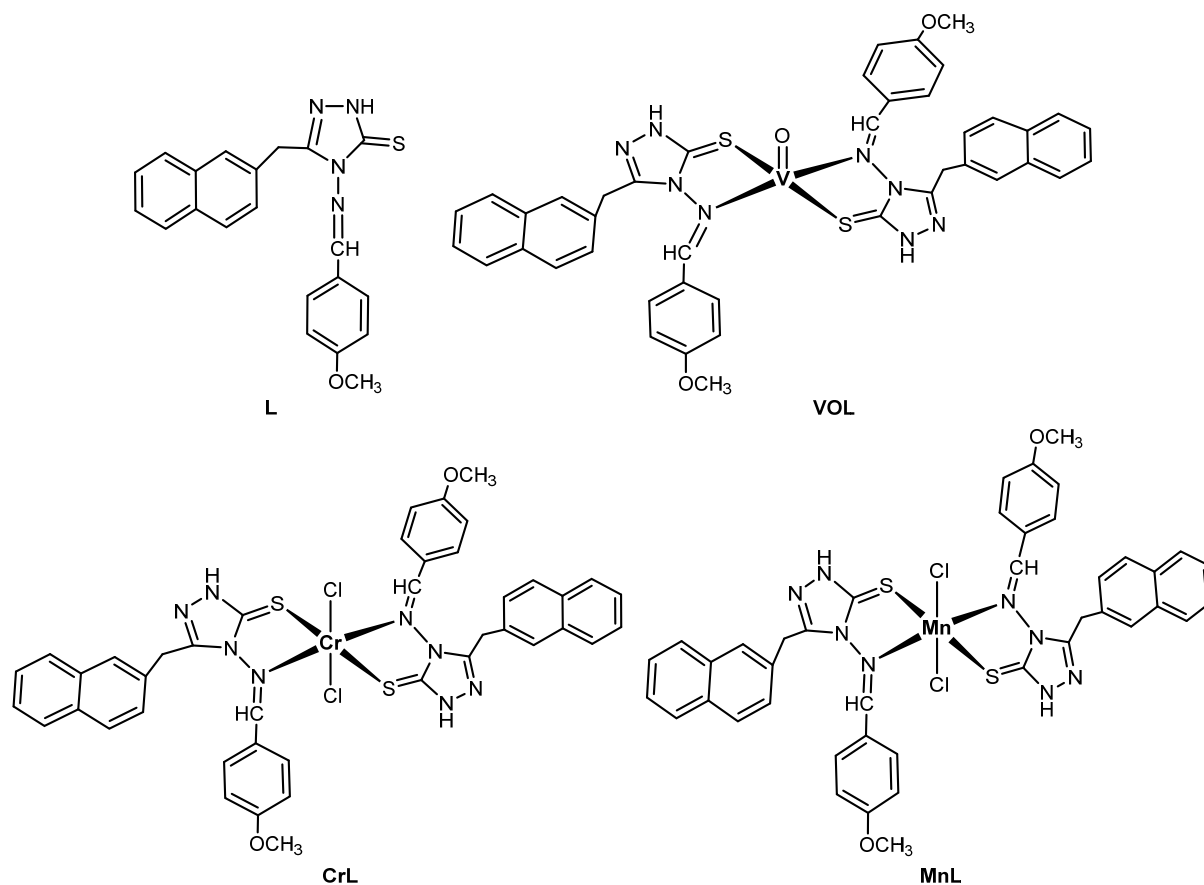


Fig 1. Stereochemical models for metal complexes with L

data, which shows that the bands are characteristic to square pyramidal geometry for vanadium(IV) were square pyramidal geometry in VO (LS) complex formula. However, the Cr(III) and Mn(II) complexes have octahedral geometry in the formulas, which closely resembles the value produced using laboratory findings.

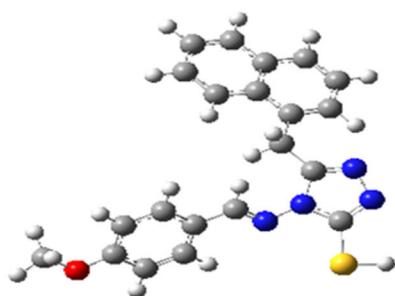
Thermodynamic parameter calculations

Similarly, single-point energy calculations were used to determine the gas-phase thermodynamic characteristics of the ligands and complexes. Based on G_{298} values, the VOL complex is the most stable of those that have been reported. The value of its G_{298} is -1575.91 kJ/mol (Table 5). The CrL complex is the second-most stable one, with a value of G_{298} of -1403.27 kJ/mol. The complex with a G_{298} value of

-1219.24 kJ/mol is the least energetic of those synthesized. We have defined the complexes formed by VOL, CrL, and MnL as “highly binding” since the values of G_{298} decrease from VOL to MnL. Analysis shows that the two-ligand complexes shown to have the strongest binding here are as stable as the synthesized complexes, and in some cases, they are even more stable. This suggests that the synthesis of these complexes is very probable.

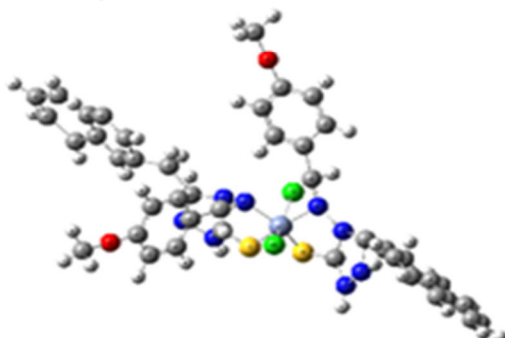
In addition, the thermodynamic parameters for the ligand and the complexes were estimated when the system was in the gas phase by doing single-point energy calculations using the same approach. VOL is the complex shown to have the least fluctuation in terms of ΔG_{298} stability compared to the other reported complexes.

E(RB3LYP) = -1502.52557020 a.u.
RMS Gradient Norm = 0.00000476 a.u.
Imaginary Freq = 0
Dipole Moment = 7.8160 Debye
Point Group = C1



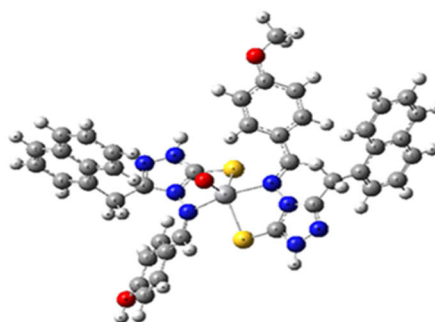
ligand

E(UB3LYP) = -4930.32102109 a.u.
RMS Gradient Norm = 0.00000369 a.u.
Imaginary Freq = 0
Dipole Moment = 6.6598 Debye
Point Group = C1



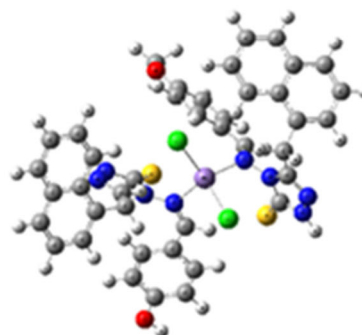
CrL

E(UB3LYP) = -3984.56387992 a.u.
RMS Gradient Norm = 0.00000153 a.u.
Imaginary Freq = 0
Dipole Moment = 7.6188 Debye
Point Group = C1



VOL

E(UB3LYP) = -5037.05293952 a.u.
RMS Gradient Norm = 0.00000492 a.u.
Imaginary Freq = 0
Dipole Moment = 8.6366 Debye
Point Group = C1



MnL

Fig 2. B3LYP/def2-SVP optimized geometries of neutral ligands and complexes

Table 4. Summarized selected bond lengths, bond angles and dihedrals calculation for all complexes

| | VOL | CrL | MnL |
|----------------------|------------------------|--------------------------------------|--------------------------------------|
| M-S bond distance | 2.41 | 2.57 | 4.51, 4.80 |
| | 2.46 | 2.57 | |
| M-N bond distance | 2.17 | 2.10 | 2.23 |
| | 2.19 | 2.18 | 2.28 |
| M specific bond | V-O 1.55 | Cr-Cl 2.12 | Mn-Cl 2.33 |
| S-M-S angle | 127.08 | 84.89 | 72.01 |
| N-M-N angle | 162.28 | 169.74 | 107.22 |
| M specific-angle | S-V-O 115.40, | Cl-Cr-Cl 93.04 | Cl-Mn-Cl 124.61 |
| | 117.35 | N-Cr-Cl 91.13, 88.18, 92.11, 101.37 | N-Mn-Cl 109.80, 99.16, 99.28, 114.66 |
| N-M-N-S dihedrals | N-V-O 100.10, 97.60 | S-Cr-Cl 92.20, 89.90, 169.96, 177.05 | S-Mn-Cl 98.80, 75.37, 128.67, 156.29 |
| | -62.94, -65.79, 90.28, | -66.12, -18.73, 18.35, 64.75 | -48.71, 30.60, -45.35, 25.51 |
| S-N-S-N | -73.74 | 64.26 | 89.77 |
| S-M-S-N dihedrals | 28.45 | -79.30, 97.41 | 99.37, -43.47 |
| M specific dihedrals | O-V-S-N -97.94, | Cl-Cr-Cl-N 88.29 | Cl-Mn-Cl-N 121.93 |
| | 114.61 | | |

Table 5. Calculated free energies (ΔG_{298K}) of L and their metal complexes

| | Zero-point energies kJ/mol | Thermal energies kJ/mol | Thermal enthalpies kJ/mol | Thermal free energies kJ/mol |
|--------|-------------------------------|----------------------------|------------------------------|---------------------------------|
| Ligand | -483.295 | -543.521 | -546.011 | -336.763 |
| VOL | -1808.78 | -1932.50 | -1934.97 | -1575.91 |
| CrL | -1643.64 | -1773.93 | -1776.41 | -1403.27 |
| MnL | -1471.41 | -1605.38 | -1607.86 | -1219.24 |

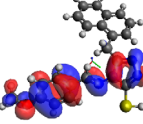
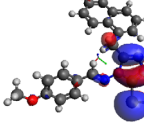
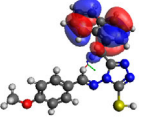
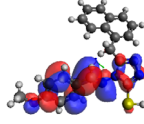
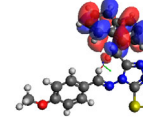
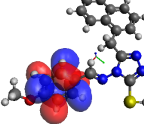
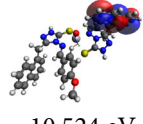
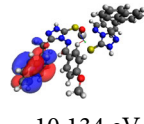
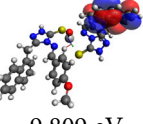
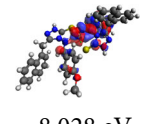
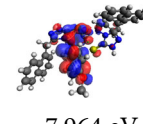
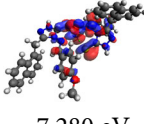
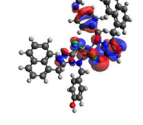
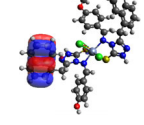
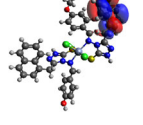
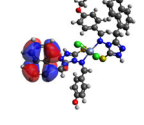
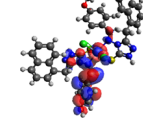

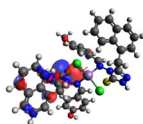

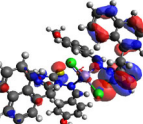
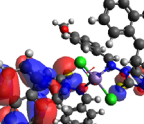
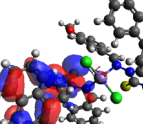
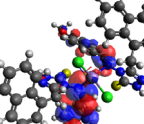
It has an ΔG_{298} value of -1575.91 kJ/mol (Table 5). The CrL complex is the next stable one, with a value of -1403.27 kJ/mol for its G_{298} energy level. The complex with the lowest value for G_{298} among those synthesized has a value of -1219.24 kJ/mol. We have considered complexes of VOL, CrL, and MnL to be “highly binding,” as shown by the fact that G_{298} values drop from VOL to MnL. Two-ligand complexes, chosen as the strongest binding complexes in this study, are shown to have stability equivalent to that of the generated complexes and, in some cases, even superior stability, demonstrating the promising potential of their synthesis.

Frontier molecular orbital analyses

The most well-known tool for assessing the stabilities of our compounds is the frontier MO analysis to recognize the distribution of electron density for these orbitals. MO analysis has been employed here to shed some light on the HOMO and the LUMO (Table 6).

Using the optimized structures of Schiff bases for MO analysis at B3LYP/def2-TZVP level of theory for single point calculation can be used as a suitable and good description for mapping orbitals distribution for the ligand and complex compounds. In addition to the figures, HOMO-2, HOMO-1, and HOMO, and LUMO, LUMO+1, and LUMO+2 energies were calculated, and the values expressed to contribute beneficial information for the chemical stability of the molecule and the orbital interactions. This result indicates a higher orbital contribution. The HOMOs, which are electronically occupied orbitals, have the preference to donate electrons, whereas the LUMOs, which are electronically empty or unoccupied orbitals, have the potential to receive electrons. A comparison of all possibilities was made depending on the energy gap values, as can be observed from Table 6, which is organized into four tetradentate chelating modes. It is

Table 6. Frontier MO for L and complexes using B3LYP/def2-TZVP

| | HOMO-2 | HOMO-1 | HOMO | LUMO | LUMO+1 | LUMO+2 |
|------|---|---|---|--|---|---|
| L |  -6.576 eV |  -6.245 eV |  -6.015 eV |  -2.200 eV |  -1.387 eV |  -1.086 eV |
| VO-L |  -10.524 eV |  -10.134 eV |  -9.809 eV |  -8.028 eV |  -7.964 eV |  -7.280 eV |
| Cr-L |  -8.735 eV |  -8.514 eV |  -8.199 eV |  -7.780 eV |  -5.198 eV |  -4.976 eV |
| Mn-L |  -6.062 eV |  -6.025 eV |  -5.929 eV |  -5.902 eV |  -5.757 eV |  -2.477 eV |

clearly perceived that the most feasible chelating sites of the ligand have been designed with two nitrogen atoms of the imine groups and two sulfur atoms of the thiol groups with central atoms due to its high stability according to the lower HOMO-LUMO energy values.

Electronegative and electropositive of specific atoms

Electronegative and electropositive atoms were determined from the MEP surface map to find the influential position of a ligand to make a stable complex. We also study charge distribution. For all complexes, the charge distribution can be found in supplementary information at the X, Y, and Z coordinates.

The Biological Activity

Representative strains of *P. aeruginosa* and *B. subtilis* were tested *in vitro* to see whether they could be inhibited by L or its metal complexes. Table 7 shows the results of the research conducted in DMSO as a solvent against *Penicillium* spp. and *A. flavus* fungi.

L has antibacterial activity against both Gram-positive and Gram-negative microorganisms. Based on the data in Table 7, all metal complexes are more effective than L against both kinds of bacteria. Table 8 shows the comparison MIC findings between the antibiotics ampicillin and amoxicillin. As shown in Table 7,

Table 7. Free ligand (L) antimicrobial activities and their metal complexes

| Compound | <i>Pseudomonas aeruginosa</i> | <i>Bacillus subtilis</i> | <i>Penicillium</i> spp. | <i>Aspergillus flavus</i> |
|--------------|-------------------------------|--------------------------|-------------------------|---------------------------|
| Control DMSO | - | - | - | - |
| L | - | - | 44 | 39 |
| VOL | 8 | 5 | 33 | 37 |
| CrL | 12 | 10 | 22 | 29 |
| MnL | 4 | 6 | 35 | 30 |

where: 6–8 (+); 8–10 (++); >10 (+++)

where: 30–40 (+++); 20–30 (++++); 10–20 (++++)

Table 8. Minimal inhibitory concentration (MIC) for L and its metal complexes ($\mu\text{g mL}^{-1}$)

| Symb. | <i>Pseudomonas aeruginosa</i> | | | | | <i>Bacillus subtilis</i> | | | | |
|-------------|-------------------------------|-------|-------|-------|-------|--------------------------|-------|-------|-------|-------|
| | 0.025 | 0.050 | 0.075 | 0.100 | 0.500 | 0.025 | 0.050 | 0.075 | 0.100 | 0.500 |
| L | + | + | + | (MIC) | - | + | + | (MIC) | - | - |
| VOL | + | (MIC) | - | - | - | + | + | (MIC) | - | - |
| CrL | (MIC) | - | - | - | - | (MIC) | - | - | - | - |
| MnL | + | + | + | + | (MIC) | + | + | + | + | (MIC) |
| Ampicillin | + | + | + | (MIC) | - | + | + | + | + | (MIC) |
| Amoxicillin | + | + | + | (MIC) | - | + | + | + | + | (MIC) |

the newly synthesized compounds exhibited increased activity even when used at relatively low concentrations. The antifungal activity findings of all of the compounds, which can be seen in Table 8, demonstrated that the metal ion chelates of the L ligand were more toxic in comparison to their parent ligand (L) when tested against the same microorganisms and under the same experimental circumstances [42].

■ CONCLUSION

The synthesized Schiff base ligand and its metal complexes were characterized utilizing a number of methods. The hypothesized structure of the Schiff base ligand and its metal complexes is consistent with the data received from numerous research. The ligand and Cr, V, and Mn complexes have been explored through theoretical computations at the UB3LYP/def2-SVP level of theory. Optimization geometries, IR frequencies, and frontier MO estimated via DFT all agree with their corresponding experimental readings. Complete data on our structures, including enthalpy, bond length, dipole moment, heat capacity, and total energy, may be supplied after validating the optimal geometries for the compounds under study. Furthermore, the theoretical results prove that the complexes with two ligands are stable enough to become isolated in a condensed phase. This study's findings show that the metals form 1:2 complexes with the ligand. It has been hypothesized that the structure of complexes has the geometry of an octahedron, except for the VO(II) complex, which has a square pyramidal shape. Studies of the complexes' antimicrobial properties demonstrate that they are more toxic than the parent ligand to the strains of bacteria and fungi used in the experiments.

■ ACKNOWLEDGMENTS

The authors would like to thank Mustansiriyah University, Baghdad, Iraq for its support in the present work. Also, the authors would like to thank the School of Chemistry, University of Southampton, UK, for providing the calculation resources.

■ AUTHOR CONTRIBUTIONS

Rehab Abdul Mahdi Al Hassani suggested the research idea and conducted the experiment. Khalidah Hamil Manati Al Furajji performed the theoretical chemistry section. Hanaa Hassan Hussein organized all the results and data and wrote and revised the manuscript. All authors agreed to the final version of this manuscript.

■ REFERENCES

- [1] Mathur, P., and Misra, S., 2020, Metal-carbonyl promoted multicomponent coupling of alkynes for the synthesis of heterocyclic compounds, *Adv. Organomet. Chem.*, 73, 253–304.
- [2] Milyushkin, A.L., Birin, K.P., Matyushin, D.D., Semeikin, A.V., Iartsev, S.D., Karnaeva, A.E., Uleanov, A.V., and Buryak, A.K., 2019, Isomeric derivatives of triazoles as new toxic decomposition products of 1,1-dimethylhydrazine. *Chemosphere*, 217, 95–99.
- [3] Brinkmann, M., Schneider, A.L., Bluhm, K., Schiwy, S., Lehmann, G., Deutschmann, B., Müller, A., Tiehm, A., and Hollert, H., 2019, Ecotoxicity of nitrogen, sulfur, or oxygen heterocycles and short-chained alkyl phenols commonly detected in contaminated groundwater, *Environ. Toxicol. Chem.*, 38 (6), 1343–1355.

- [4] Dwivedi, A., Singh, S., Kumar, S., and Mittal, P.C., 2020, "Chapter 11 - Organosulfur Phytochemicals against Metabolic and Neurodegenerative Diseases: Benefits and Risks" in *Phytochemicals as Lead Compounds for New Drug Discovery*, Eds. Egbuna, C., Kumar, S., Ifemeje, J.C., Ezzat, S.M., and Kaliyaperumal, S., Elsevier, Amsterdam, Netherlands, 179–194.
- [5] Fayyadh, B.M., Jaafar, W.A., and Sarhan, B.M., 2021, Synthesis, structural study, and biological activity evaluation of VO(II), Mn(II), Co(II), Ni(II), Cu(II), Zn(II), Cd(II), and Hg(II) complexes with new Schiff base ligand derived from pyrazine, *Int. J. Drug Delivery Technol.*, 11 (1), 64–69.
- [6] Raouf, H., Beyramabadi, S.A., Allameh, S., and Morsali, A., 2019, Synthesis, experimental and theoretical characterizations of a 1,2,4-triazole Schiff base and its nickel(II) complex, *J. Mol. Struct.*, 1179, 779–786.
- [7] Koga, N., and Morokuma, K., 1991, *Ab initio* molecular orbital studies of catalytic elementary reactions and catalytic cycles of transition-metal complexes, *Chem. Rev.*, 91 (5), 823–842.
- [8] Musaev, D.G., and Morokuma, K., 1996, "Advances in chemical physics" in *Advances in Chemical Physics*, Eds. Prigogine, I., and Rice, S.A., John Wiley & Sons, New York, US, 61–128.
- [9] Siegbahn, P.E.M., and Blomberg, M.R.A., 1995, "Oxidative Addition Reactions" in *Theoretical Aspects of Homogeneous Catalysis: Applications of Ab Initio Molecular Orbital Theory*, Eds. Van Leeuwen, P.W.N.M., Morokuma, K., and Van Lenthe, J.H., Editors, Springer, Dordrecht, Netherlands, 15–63.
- [10] Salahub, D.R., Castro, M., Fournier, R., Calaminici, P., Godbout, N., Goursot, A., Jamorski, C., Kobayashi, H., Martínez, A., Pápai, I., Proynov, E., Russo, N., Sirois, S., Ushio, J., and Vela, A., 1994, "Density Functional Description of Metal-Metal and Metal-Ligand Bonds" in *Theoretical and Computational Approaches to Interface Phenomena*, Eds. Sellers, H.L., and Golab, J.T., Springer US, Boston, MA, 187–218.
- [11] Ellouz, M., Sebbar, N.K., Fichtali, I., Ouzidan, Y., Mennane, Z., Charof, R., Mague, J.T., Urrutigoity, M., and Essassi, E.M., 2018, Synthesis and antibacterial activity of new 1,2,3-triazolylmethyl-2H-1,4-benzothiazin-3(4H)-one derivatives, *Chem. Cent. J.*, 12 (1), 123.
- [12] Karpun, Y., Parchenko, V., Fotina, T., Demianenko, D., Fotin, A., Nahorny, V.V., and Nahorna, N., 2021, The investigation of antimicrobial activity of some S-substituted bis-1,2,4-triazole-3-thiones, *Pharmacia*, 68 (4), 721–730.
- [13] Tratrát, C., Haroun, M., Papisova, A., Geronikaki, A., Kamoutsis, C., Ćirić, A., Glamočlija, J., Soković, M., Fotakis, C., Zoumpoulakis, P., Bhunia, S.S., and Saxena, A.K., 2018, Design, synthesis and biological evaluation of new substituted 5-benzylideno-2-adamantylthiazol[3,2-b][1,2,4]triazol-6(5H)ones. Pharmacophore models for antifungal activity, *Arabian J. Chem.*, 11 (4), 573–590.
- [14] Othman, A.A., Kihel, M., and Amara, S., 2019, 1,3,4-Oxadiazole, 1,3,4-thiadiazole and 1,2,4-triazole derivatives as potential antibacterial agents, *Arabian J. Chem.*, 12 (7), 1660–1675.
- [15] Matsuzaki, H., Takeda, N., Yasui, M., Okazaki, M., Suzuki, S., and Ueda, M., 2021, Synthesis of multi-substituted 1,2,4-triazoles utilizing the amphiphilic reactivity of hydrazones, *Chem. Commun.*, 57 (91), 12187–12190.
- [16] Aswathanarayanappa, C., Bheemappa, E., Bodke, Y.D., Krishnegowda, P.S., Venkata, S.P., and Ningegowda, R., 2013, Synthesis and evaluation of antioxidant properties of novel 1,2,4-triazole-based Schiff base heterocycles, *Arch. Pharm.*, 346 (12), 922–930.
- [17] Al-Mansury, S., Balakit, A.A., Alkazazz, F.F., Madlum, K.N., and Ghaleb, R.A., 2019, Synthesis and anti-colon cancer activity of 1,2,4-triazole derivatives with aliphatic S-substituents, *Orient. J. Chem.*, 35 (1), 77–84.
- [18] Al-Khazraji, A.M.A., Al Hassani, R.A.M., and Ahmed, A., 2020, Studies on the photostability of polystyrene films with new metals complex of 1,2,4-

- triazole-3-thione derivate, *Syst. Rev. Pharm.*, 11 (5), 525–534.
- [19] Zein, N., Shaban, S.M., Shafek, S.H., Baghi, H., Aiad, I., and Omran, M., 2021, Synthesis and characterization of new 1,2,4-triazole anticancer scaffold derivatives: *In vitro* study, *Egypt. J. Chem.*, 64 (8), 4005–4015.
- [20] Deodware, S.A., Barache, U.B., Chanshetti, U.B., Sathe, D.J., Panchsheela Ashok, U., Gaikwad, S.H., and Prasad Kollur, S., 2021, Newly synthesized triazole-based Schiff base ligands and their Co(II) complexes as antimicrobial and anticancer agents: Chemical synthesis, structure and biological investigations, *Results Chem.*, 3, 100162.
- [21] Peng, Z., Wang, G., Zeng, Q.H., Li, Y., Wu, Y., Liu, H., Wang, J.J., and Zhao, Y., 2021, Synthesis, antioxidant and anti-tyrosinase activity of 1,2,4-triazole hydrazones as antibrowning agents, *Food Chem.*, 341 (Part 2), 128265.
- [22] Bader, A.T., Al-qasii, N.A.R., Shntaif, A.H., El Marouani, M., AL Majidi, M.I.H., Trif, L., and Boulhaoua, M., 2022, Synthesis, structural analysis and thermal behavior of new 1,2,4-triazole derivative and its transition metal complexes, *Indones. J. Chem.*, 22 (1), 223–232.
- [23] Al-Alzawi, S.M., Al-Jibouri, M.N., Rasheed, A.M., and Al-Bayati, S.M., 2023, Synthesis, characterization and antimicrobial activity of complexes metal ions Ni(II), Zn(II), Pd(II) and Pt(IV) with polydentate 1,2,4-triazole ligand, *Indones. J. Chem.*, 23 (1), 210–218
- [24] Frisch, M.J., Trucks, G.W., Schlegel, H.B., Scuseria, G.E., Robb, M.A., Cheeseman, J.R., Scalmani, G., Barone, V., Mennucci, B., Petersson, G.A., Nakatsuji, H., Caricato, M., Li, X., Hratchian, H.P., Izmaylov, A.F., Bloino, J., Zheng, G., Sonnenberg, J.L., Hada, M., Ehara, M., Toyota, K., Fukuda, R., Hasegawa, J., Ishida, M., Nakajima, T., Honda, Y., Kitao, O., Nakai, H., Vreven, T., Montgomery, J.A., Jr., Peralta, J.E., Ogliaro, F., Bearpark, M., Heyd, J.J., Brothers, E., Kudin, K.N., Staroverov, V.N., Kobayashi, R., Normand, J., Raghavachari, K., Rendell, A., Burant, J.C., Iyengar, S.S., Tomasi, J., Cossi, M., Rega, N., Millam, J.M., Klene, M., Knox, J.E., Cross, J.B., Bakken, V., Adamo, C., Jaramillo, J., Gomperts, R., Stratmann, R.E., Yazyev, O., Austin, A.J., Cammi, R., Pomelli, C., Ochterski, J.W., Martin, R.L., Morokuma, K., Zakrzewski, V.G., Voth, G.A., Salvador, P., Dannenberg, J.J., Dapprich, S., Daniels, A.D., Farkas, Ö., Foresman, J.B., Ortiz, J.V., Cioslowski, J., and Fox, D.J., 2016, *Gaussian 16, Revision C.01*, Gaussian, Inc., Wallingford, CT.
- [25] Lu, L., 2015, Can B3LYP be improved by optimization of the proportions of exchange and correlation functionals?, *Int. J. Quantum Chem.*, 115 (8), 502–509.
- [26] Al Furaiji, K.H.M., Molino, A., Dutton, J.L., and Wilson, D.J.D., 2020, Theoretical investigation of main-group element hydride insertion into phosphorus-heterocyclic carbenes (PHCs), *Aust. J. Chem.*, 73 (8), 787–793.
- [27] Berger, R., 2016, Computational chemistry. Introduction to the theory and applications of molecular and quantum mechanics. Von Errol G. Lewars, *Angew. Chem.*, 116 (38), 5087–5089.
- [28] Cheng, G.J., Zhang, X., Chung, L.W., Xu, L., and Wu, Y.D., 2015, Computational organic chemistry: Bridging theory and experiment in establishing the mechanisms of chemical reactions, *J. Am. Chem. Soc.*, 137 (5), 1706–1725.
- [29] Koch, W., and Holthausen, M.C., 2015, *A Chemist's Guide to Density Functional Theory*, 2nd Ed., John Wiley & Sons, Weinheim, Germany.
- [30] Lee, C., Yang, W., and Parr, R.G., 1988, Development of the Colle-Salvetti correlation-energy formula into a functional of the electron density, *Phys. Rev. B: Condens. Matter Mater. Phys.*, 37 (2), 785–789.
- [31] Al Furaiji, K.H.M., Iversen, K.J., Dutton, J.L., and Wilson, D.J.D., 2018, Theoretical investigation of hydride insertion into *N*-heterocyclic carbenes containing N, P, C, O and S heteroatoms, *Chem. - Asian J.*, 13 (23), 3745–3752.
- [32] Lever, A.B.P., 1984, *Inorganic Electronic Spectroscopy*, Elsevier, Amsterdam.
- [33] Zhang, J., Wang, S., Ba, Y., and Xu, Z., 2019, 1,2,4-Triazole-quinoline/quinolone hybrids as potential anti-bacterial agents, *Eur. J. Med. Chem.*, 174, 1–8.

- [34] Patil, B.S., Krishnamurthy, G., Shashikumar, N.D., Lokesh, M.R., and Bhojya Naik, H.S., 2013, Synthesis and antimicrobial activity of some [1,2,4]-triazole derivatives, *J. Chem.*, 2013, 462594.
- [35] Barot, K.P., Manna, K.S., and Ghate, M.D., 2017, Design, synthesis and antimicrobial activities of some novel 1,3,4-thiadiazole, 1,2,4-triazole-5-thione and 1,3-thiazolan-4-one derivatives of benzimidazole, *J. Saudi Chem. Soc.*, 21, S35–S43.
- [36] Dilmaghani, K.A., Pur, F.N., and Nezhad, M.H., 2015, Synthesis and antibacterial evaluation of new thione substituted 1,2,4-triazole Schiff bases as novel antimicrobial agents, *Iran. J. Pharm. Res.*, 14 (3), 693–699.
- [37] Al-Hassani, R.A.M., 2016, Synthesis, structural, antimicrobial activities and theoretical studies of some new trivalent metal complexes with thiocarbamide derivative, *Int. J. ChemTech Res.*, 9 (5), 723–737.
- [38] Al-Hassani, R.A.M., and Shaheen, E.S.K., 2013, Synthesis, characterization, theoretical studies and bioactivity of Mn(II), Co(II), Ni(II), Cu(II) and Zn(II) complexes with Mannich base and tryptophane as mixed ligand, *Asian J. Biochem. Pharm. Res.*, 3 (1), 1–27.
- [39] Carlin, R.L., and van Duyneveldt, A.J., 1977, *Magnetic Properties of Transition Metal Compounds*, Springer-Verlag, New York, US.
- [40] Greenwood, N.N., and Earnshaw, A., 1998, *Chemistry of the Elements*, 2nd Ed., Butterworth-Heinemann, Oxford, UK.
- [41] Figgis, B.N., and Hitchman, M.A., 1999, *Ligand Field Theory and Its Applications*, 1st Ed., Wiley-VCH, Weinheim, Germany.
- [42] Hussein, H.H., Hussein, F.M., Mohammed, E.Z., and Askar, F.W., 2020, Synthesis, characterization and theoretical study of 2-(2-(thiophen-2-yl)-1H-benzo[d]imidazole-1-yl) acetohydrazide and its complexes, *Int. J. Pharm. Res.*, 12 (2), 1233–1242.